

Rotational-hyperfine cooling of ^{205}TlF in a cryogenic beam

Olivier Grasdijk* and David DeMille†

Physics Division, Argonne National Laboratory, Argonne, IL 60439, United States of America

Jakob Kastelic, Steve Lamoreaux, and Oskari Timgren

Department of Physics, Yale University, New Haven, CT 06511, United States of America

Konrad Wenz and Tanya Zelevinsky

Department of Physics, Columbia University, New York, NY 10027-5255, United States of America

David Kwall

*Department of Physics, University of Massachusetts Amherst,
Amherst, MA 01003, United States of America*

(CeNTREX Collaboration)

(Dated: January 13, 2025)

The aim of CeNTREX (Cold Molecule Nuclear Time-Reversal Experiment) is to search for time-reversal symmetry violation in the thallium nucleus, by measuring the Schiff moment of ^{205}Tl in the polar molecule thallium fluoride (TlF). CeNTREX uses a cryogenic beam of TlF with a rotational temperature of 6.3(2) K. This results in population spread over dozens of rotational and hyperfine sublevels of TlF, while only a single level is useful for the Schiff moment measurement. Here we present a protocol for cooling the rotational and hyperfine degrees of freedom in the CeNTREX beam, transferring the majority of the Boltzmann distribution into a single rotational and hyperfine sublevel by using a single ultraviolet laser and a pair of microwave beams. We achieve a factor of 20.1(4) gain in the population of the $J = 0, F = 0$ hyperfine sublevel of the TlF ground state.

I. INTRODUCTION

CeNTREX (Cold Molecule Nuclear Time-Reversal Experiment) aims to achieve a significant increase in sensitivity over the best present upper bounds on the strength of certain hadronic time-reversal (T) violating fundamental interactions such as the proton's electric dipole moment and the CP -violating parameter of quantum chromodynamics, θ_{QCD} . The overall approach of CeNTREX, and details of its measurement strategy, are described in [1]. CeNTREX seeks to determine the Schiff moment of the ^{205}Tl nucleus by performing magnetic resonance measurements on the nucleus within an electrically polarized thallium monofluoride (TlF) molecule. The strongly polarized electron shells in the molecule interact strongly with the Schiff moment, providing orders of magnitude larger shifts of the magnetic resonance frequency than in experiments using atoms, for the same size of Schiff moment [2].

CeNTREX makes use of a cryogenic buffer gas cooled molecular beam source [1, 3] to create a beam of TlF. This source delivers a beam with high intensity (for good statistics), low mean velocity (to enable long interaction time and good energy resolution), low velocity dispersion (to enable efficient electrostatic focusing [4]) and low rotational temperature (to reduce the spread of population

over many internal states). The CeNTREX source uses a neon buffer gas at a temperature of 19 K. Compared to colder sources using helium buffer gas, this allows operation at higher repetition rates and gives steadier flux of very heavy species [5] such as TlF.

After some cooling during the free expansion of the neon gas as it exits the source, the TlF has a rotational temperature $T_{\text{rot}} = 6.3(2)$ K [1]. At this temperature, only $\sim 5\%$ of the TlF molecules are in the lowest rotational level $J = 0$ (where J is the rotational quantum number), and only 1/4 of these are in the absolute hyperfine/rotational ground state $J = 0, F = 0$ [where F is the total hyperfine angular momentum including rotation and the nuclear spins of ^{205}Tl ($I_1 = 1/2$) and ^{19}F ($I_2 = 1/2$)]. Only this single sublevel is used for the Schiff moment measurement protocol in CeNTREX [1].

Here we describe a method to dramatically increase the population of this level, and hence to improve the statistical sensitivity of the experiment. We refer to our method as rotational/hyperfine cooling of the TlF molecules. While rotational cooling has been previously performed in molecules and molecular ions [6, 7], it has not been done for hyperfine structure or a closed-shell molecule before. Using a combination of laser optical pumping and microwave-driven rotational state transfer, we drive most of the population from all hyperfine sublevels of the three lowest excited rotational levels ($J = 1, 2$, and 3) into the $J = 0$ manifold of states, preferentially into the $F = 0$ sublevel. In the Boltzmann distribution at $T_{\text{rot}} = 6.3(2)$ K, approximately 56% of the population is in the lowest four rotational states, i.e. $J = 0 - 3$. If all population in the $J = 0, 1, 2$,

* jgrasdijk@argonne.gov

† Joint appointment at the Department of Physics, University of Chicago, Chicago, IL 60637, United States of America

and 3 rotational ground states were transferred to the $|J = 0, F = 0\rangle$ state, a maximum gain of ≈ 45 in its population could be achieved. Though our method incorporates a simplification that reduces the maximum potential gain to ≈ 29 , this enhancement in signal size for the ^{205}Tl Schiff moment measurement is crucial for CeNTREX to attain its projected sensitivity [1].

In what follows, we explain the principle of our method for rotational/hyperfine cooling of TlF, and present experimental results on its implementation.

II. PRINCIPLE OF THE METHOD

To explain our method, we first review relevant aspects of the structure of TlF (see e.g. [1] for more details). Throughout, unless otherwise noted, we discuss only states with vibrational quantum number $v = 0$. The ground state X $^1\Sigma^+$ has a rotational constant $B = 6.66733$ GHz and nominal rotational energies $E_J = BJ(J+1)$. The ^{205}Tl and ^{19}F nuclear spins give rise to hyperfine substructure in the rotational states. The lowest rotational state, $|J = 0\rangle$, splits into two levels, with $F = 0$ and $F = 1$. All higher rotational states split into four hyperfine states, with $F = J+1, J, J,$ and $J-1$. Hyperfine splittings in the low- J levels of interest here are always less than 600 kHz. In the $J = 0$ state, $F = 1$ is split from $F = 0$ by only 13 kHz. Transitions between states with $\Delta J = \pm 1$ can be coupled with microwave electromagnetic fields.

The dissipation required for our rotational/hyperfine cooling scheme comes from spontaneous emission in an optical transition. We perform optical pumping by exciting a transition from the ground state to the B $^3\Pi_1$ excited state, using a laser at 271.75 nm. The B $^3\Pi_1$ state has a natural width $\Gamma_B = 2\pi \times 1.6$ MHz, so the ground state hyperfine structure is completely unresolved in the optical transition. However, the B $^3\Pi_1$ state has very large hyperfine splittings, so the laser addresses a single hyperfine level in the excited state. Each such state can be described in terms of quantum numbers $J', F'_1 = J' + I_1, F' = F'_1 + I_2$, and parity P' . However, the hyperfine interaction in the excited state is so strong that states with quantum numbers J' and F'_1 can be strongly mixed; we indicate the approximate nature of these quantum numbers by labeling them \tilde{J}' and \tilde{F}'_1 . Branching ratios for decays of these excited-state hyperfine/rotational levels are compiled in Ref. [8].

Rotational/hyperfine cooling is accomplished with a single optical pumping laser and two microwave driving fields. The $J = 2$ ground state is coupled with the laser to the $|\tilde{J}'^P = 1^-, \tilde{F}'_1 = 3/2, \tilde{F}' = 1\rangle$ excited state, as shown in Fig. 1(a). We refer to this P -branch transition (with $\tilde{J}' = J-1$) as the $P2 F1$ transition. Roughly half the decays from $\tilde{J}' = 1$ end up in the $J = 0$ ground state, and nearly all of the remainder returns to $J = 2$; the only loss is from branching to other vibrational states which amounts to $\lesssim 1\%$ [9–11]. Simultaneous with the laser

excitation, resonant microwaves couple the $J = 1 \leftrightarrow 2$ and $J = 2 \leftrightarrow 3$ transitions. Repeated excitation-decay cycles accumulate population from $J = 1, 2, 3$ into the $J = 0$ state.

In the decay of $|\tilde{J}'^P = 1^-, \tilde{F}'_1 = 3/2, \tilde{F}' = 1\rangle$ into $|J = 0\rangle$, branching ratios dictate that nearly 70% of the time the $|J = 0, F = 0\rangle$ sublevel is populated. We rely only on this effect to enhance the population of the $F = 0$ level relative to $F = 1$ as shown in Fig. 1(b). (Note that in thermal equilibrium, the $F = 1$ level has three times the population of $F = 0$.) With this scheme and the known rotational temperature, a maximum gain of 29.4(3) in the $|J = 0, F = 0\rangle$ population can be expected for a full depletion of the $J = 1, 2,$ and 3 rotational ground states.

The particular hyperfine structure of TlF adds substantial complexity to the hyperfine/rotational cooling process. Exciting a single excited-state hyperfine level with the laser, while also coupling many unresolved hyperfine states in the ground state rotational manifold, leads to a low excitation and pumping rate due to the formation of long-lived coherent dark states [12]. In our scheme, we work to rapidly destabilize the dark states by switching polarizations of both microwave excitation fields [13, 14] and by ensuring that no pair of the three excitation fields (two microwave plus one laser) are either parallel or perpendicular to each other. The photon scattering rate on the laser-driven transition, Γ_{sc} , is bounded by $\Gamma_{sc} \lesssim \Gamma_B \cdot n_e / (n_g + n_e)$ [15], where $n_e = 3$ is the number of excited state sublevels and $n_g = 60$ is the number of simultaneously coupled ground-state sub-levels. This reduction in scattering rate means that substantial interaction time is needed to achieve efficient optical pumping. To accomplish this while maintaining sufficient laser intensity to maximize the excited-state population, we send multiple passes of the laser beam through the molecular beam.

In CeNTREX, following the rotational/hyperfine cooling region, an electrostatic quadrupole lens is used to collimate the molecular beam. The lens accepts transverse velocities $|v_{\perp}| < v_{\perp}^{\max} = 2$ m/s. Hence, a key requirement for the rotational/hyperfine cooling is that it be effective over this full range of transverse velocities. This corresponds to a range of Doppler shifts, $\pm\delta_D^{\max}$, that is much larger than the natural width of the transition: $\delta_D^{\max} \approx 4.7\Gamma_B$. Therefore, substantial spectral broadening of the optical pumping light is necessary.

III. EXPERIMENTAL SETUP

A. Overview

A schematic of the setup is shown in Figure 2. The TlF cryogenic beam, traveling horizontally with mean forward velocity $\bar{v}_f = 184$ m/s, enters a chamber where the rotational cooling takes place, at a distance of approximately 40 cm from the beam source and 60 cm from

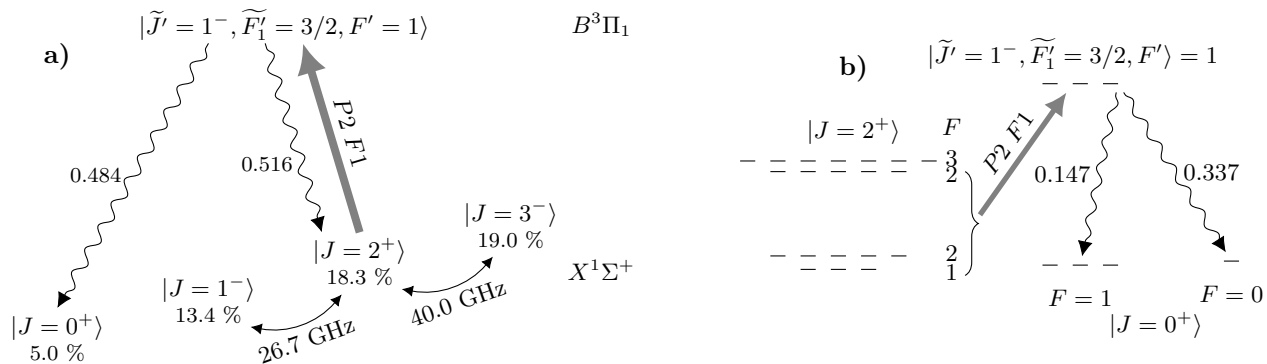


FIG. 1. Rotational cooling scheme. **a**. The thick solid arrow denotes a UV laser driving the $P2 F1$ transition; bent arrows represent microwaves, and wavy arrows indicate spontaneous emission with branching ratios as indicated. The odd-parity $\tilde{J}' = 1^-$ excited state can only decay to states with $J = 0^+, 2^+$. Percentages under the ground-state kets are the thermal population at temperature $T_{\text{rot}} = 6.3\text{ K}$, prior to rotational cooling. **b**. Hyperfine structure relevant to optical pumping. Decays back to $J = 2^+$ are not shown. While the $P2 F1$ transition does not excite $|J = 2^+, F = 3\rangle$, this level can be coupled into the system by microwave-induced transfer to the $|J = 3^-, F = 2, 3\rangle$ levels and subsequent stimulated emission to $|J = 2^+, F = 1, 2\rangle$. Figure taken from [1].

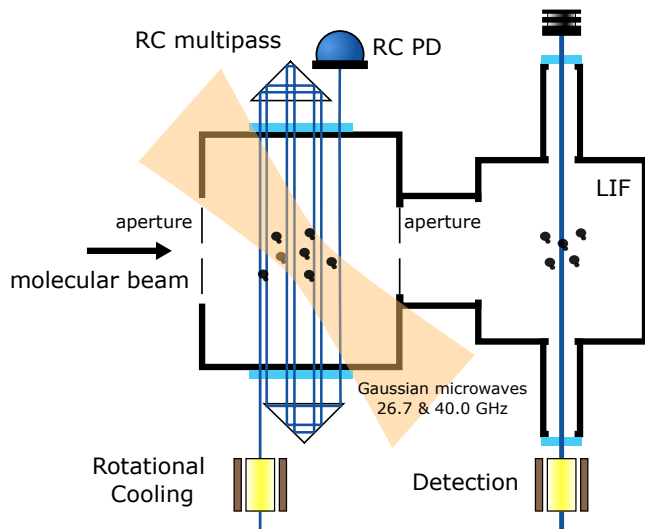


FIG. 2. Schematic overview of the rotational cooling (RC) gain measurement. Two circular apertures with 8 mm diameter constrict the transverse velocity and spread of the molecular beam. A 271.75 nm laser at the $P(2) \tilde{F}'_1 = 3/2 F' = 1$ transition is phase modulated and passed 13 times through the rotational cooling region, where it intersects with two focused Gaussian microwave beams. The populations are read out with laser-induced fluorescence (LIF) captured in a photomultiplier tube (PMT) from a single phase-modulated laser beam at 271.75 nm.

the cell exit. Here, the molecular beam is crossed simultaneously by a multi-passed laser beam and two focused, free-space microwave beams, which all serve to perform the rotational/hyperfine cooling. These beams are all nominally orthogonal to the molecules' trajectories and at 33° angles w.r.t. each other; they are shaped so as to cover the entire vertical transverse extent of the collimated molecular beam which is a circle of 8 mm diameter.

The polarization of each microwave beam and the laser beam can be alternated between two orthogonal linear directions. Polarization switching makes it possible to address all hyperfine/Zee-man sublevels in the rotational state manifolds. If the switching is sufficiently rapid (at angular frequency ω such that $\omega \gtrsim \Omega_\mu$ or Γ_B , where Ω_μ is the maximum Rabi frequency of the driven microwave transitions), it also can disrupt formation of dark states [12] that could otherwise slow the optical pumping rate.

After this interaction region, the molecules travel downstream ~ 40 cm to a detection region. Here a probe laser, again propagating orthogonal to the molecular trajectories, is tuned to excite molecules in selected sublevels (see below). A photomultiplier, placed orthogonally to both the molecule and probe laser beams, detects the laser-induced $B - X$ fluorescence.

B. Rotational cooling laser

The $P(2) \tilde{F}'_1 = 3/2 F' = 1$ optical transition [9, 10] is at wavelength 271.75 nm. The ultraviolet (UV) laser light is generated from frequency quadrupled 1087 nm light, using two successive second-harmonic generation (SHG) stages. A fiber seed laser is fiber-amplified to 1.5 W. Resonant-cavity SHG generates 700 mW of 543.5 nm light, which is fiber coupled and subsequently frequency doubled with another resonant-cavity SHG setup to produce ~ 90 mW of 271.75 nm light. The resulting UV laser beam is then electro-optically phase modulated at angular frequency $\omega = \Gamma_B$ with modulation parameter $\beta = 3.8$, to generate a spectral pattern containing substantial power in the carrier and all sidebands up to the 5th order; this covers the entire range of Doppler broadening up to $\pm \delta_D^{\text{max}}$. An additional electro-optical modulator was used to rapidly switch the laser polarization for some measurements.

A pair of cylindrical lenses vertically expands the UV laser beam to a $1/e^2$ diameter of 1 cm, while its horizontal diameter is 2 mm. Two identical right-angle prisms, placed horizontally on either side of the molecular beam at the same height, are oriented with their $\sqrt{2}$ -inch long hypotenuses parallel to the molecular beam forward velocity. Their positions are offset along the direction of the molecular beam by 8 mm, so that a beam input on the uncovered edge of one prism makes 13 passes through the molecular beam before exiting the open edge of the other prism. This multipass geometry of the laser beam extends the interaction time with the molecules to $\sim 210 \mu\text{s}$ while maintaining a high intensity as needed for efficient optical pumping. Losses in the optical path cause the intensity of the laser to reduce by a factor of ~ 8 from the first to the last pass. The average intensity seen by the molecules is $\sim 79 \text{ mW}/\text{cm}^2$. Here the average intensity is calculated from the $1/e^2$ intensity point of the first pass to the $1/e^2$ point of the last pass along the beam direction, and vertically by the accepted trajectories (which cover approximately $\pm 3.5 \text{ mm}$ from the beam center).

C. Microwave generation and delivery

The rotational ground states, separated by several tens of GHz, are coupled via microwave electric fields. The $J = 1 \leftrightarrow J = 2$ transition has a resonant frequency of 26.6 GHz, and the $J = 2 \leftrightarrow J = 3$ transition is at 40.0 GHz. A schematic of the microwave systems is given in Fig. 3. A source signal at 13.3 GHz from a synthesizer is frequency doubled (quadrupled) to produce 26.6(40.0) GHz. These microwaves are amplified, then delivered to the interaction region using cylindrically symmetric spot-focusing lens antennas, fed via circular waveguides. These provide free-space microwave beams, focused with -3 dB diameters of 2.54 cm at the position of the molecules. The microwaves enter and exit the vacuum chamber via fused silica windows. The maximum intensity at the molecules' position is $\sim 34 \text{ mW}/\text{cm}^2$. The polarization of the microwave beams is rapidly switched between two orthogonal linear polarizations as shown in Fig. 3.

D. Detection laser

Like the $P(2) \tilde{F}'_1 = 3/2 F' = 1$ rotational cooling transition, the $R(0) \tilde{F}'_1 = 1/2 F' = 1$ and $R(0) \tilde{F}'_1 = 3/2 F' = 2$ detection transitions are also at wavelength 271.75 nm (see below for more details). The UV laser is generated equivalently to the rotational cooling laser (Sec. III B), producing 35 mW and expanded to a $1/e^2$ diameter of 6.5 mm, which results in a peak intensity of $240 \text{ mW}/\text{cm}^2$. Similarly to the rotational cooling laser, this UV laser beam is electro-optically phase modulated at angular frequency $\omega = \Gamma_B$ with modulation parameter $\beta = 3.8$ to cover the Doppler broadening. An addi-

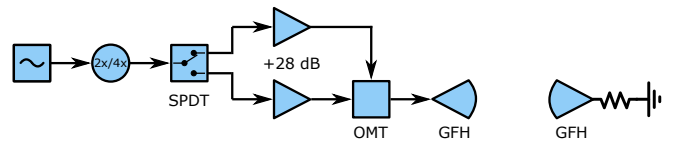


FIG. 3. Schematic overview of the frequency doubled or quadrupled microwave generation system. Identical Gaussian focusing horn (GFH) lens antennas capture and terminate the microwave beams after they traverse the interaction region, to minimize reflections. The linear polarization of the microwave beams is alternated with a single-pole double-throw (SPDT) switch that directs the input microwaves through one of two circuit branches; each branch is amplified, then fed to one of the two orthogonally-polarized inputs of an orthomode transducer (OMT) whose circular-waveguide output feeds the transmitting GFH antenna.

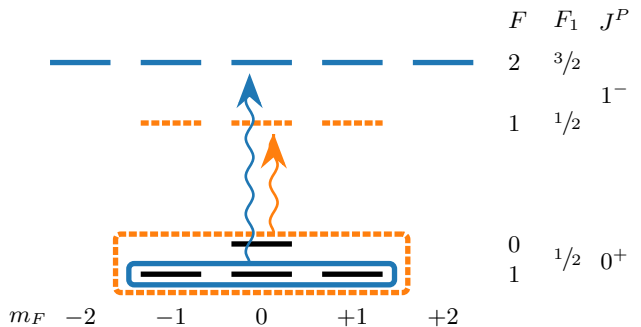


FIG. 4. Detection transitions used to calculate the gain. The $R(0) \tilde{F}'_1 = 3/2 F' = 2$ transition (blue, solid) has no dark states and easily saturates. The $R(0) \tilde{F}'_1 = 1/2 F' = 1$ transition (orange, dashed) has dark states causing an imbalance in the relative amount of photons coming from the $F = 0$ and $F = 1$ ground state levels.

tional EOM modulates the polarization at angular frequency $\omega = \Gamma_B$ to destabilize dark states in the case of $R(0) \tilde{F}'_1 = 1/2 F' = 1$.

E. Gain measurement schemes

The figure of merit for the rotational/hyperfine cooling is the gain in population of the $|J = 0, F = 0\rangle$ state. It is difficult to directly probe the population of this state. The optical transition linewidth is much larger than the hyperfine splitting in the ground state, and there is no optical transition where selection rules ensure excitation only of the $|J = 0, F = 0\rangle$ state; hence, every probe of the $J = 0$ state inevitably also addresses the $|J = 0, F = 1\rangle$ state.

To extract information about the population gain in the $|J = 0, F = 0\rangle$ state, we use several schemes. These are in principle equivalent, but sensitive to different systematic errors and hence provide a useful cross-check of the indirect probes. These schemes use two optical probe transitions, which we denote as $R(0) \tilde{F}'_1 = 3/2 F' = 2$

and $R(0) \tilde{F}'_1 = 1/2 F' = 1$ as shown in Fig. 4, to determine population in various sublevels of the $J = 0$ state. The $R(0) \tilde{F}'_1 = 3/2 F' = 2$ transition excites molecules only from the $F = 1$ hyperfine level of the $J = 0^+$ ground state, to the excited state with $J' = 1^-, F'1' = 3/2, F' = 2$. All Zeeman sublevels ($m_F = 0, \pm 1$) are excited with any polarization of light. We refer to the fluorescence signal when probing on this transition as S_1 . The $R(0) \tilde{F}'_1 = 1/2 F' = 1$ transition excites from the unresolved $F = 0$ and $F = 1$ hyperfine levels of the $J = 0^+$ ground state, to the excited state with $J' = 1^-, F'1' = 1/2, F' = 1$. With the probe light rapidly modulated between orthogonal linear polarizations, this transition can excite population from all Zeeman sublevels of both the $F = 0$ and $F = 1$ levels. We refer to the fluorescence signal when probing on this transition as S_{0+1} .

With these signals, we use the following schemes to deduce the gain in the $|J = 0, F = 1\rangle$ state population:

- Scheme 1: $R(0) \tilde{F}'_1 = 3/2 F' = 2$ branching ratio method. Here we use S_1 to detect the total population in the $|J = 0, F = 1\rangle$ level, with rotational cooling on (S_1^{on}) and off (S_1^{off}). Then the gain in the population of the $|J = 0, F = 1\rangle$ level, G_1 , is

$$G_1 \equiv \frac{S_1^{\text{on}}}{S_1^{\text{off}}}. \quad (1)$$

If the initial population in the $|J = 0, F = 1\rangle$ level is ρ_1 , the change in its population due to rotational cooling, $\Delta\rho_1$, is

$$\Delta\rho_1 = (G_1 - 1)\rho_1 = 3(G_1 - 1)\rho_0, \quad (2)$$

where we use the fact that the initial (thermal) population in the $|J = 0, F = 0\rangle$ level, ρ_0 , is $1/3$ of ρ_1 . The change in population of the $|J = 0, F = 0\rangle$ level, $\Delta\rho_0$, is given by

$$\Delta\rho_0 = \frac{br_{F=0}}{br_{F=1}} \Delta\rho_1, \quad (3)$$

where $br_{F=0}$ ($br_{F=1}$) is the branching ratio for decay from the $J' = 1^-, F'1' = 3/2, F' = 1$ excited state of the rotational cooling transition, into the $J = 0, F = 0$ ($F = 1$) level.

Finally, the gain in population of the $|J = 0, F = 0\rangle$ level, G_0 , is then given by:

$$G_0^{(1)} = \frac{\Delta\rho_0}{\rho_0} + 1 = 3 \frac{br_{F=0}}{br_{F=1}} (G_1 - 1) + 1, \quad (4)$$

where the superscript refers to the number of the scheme.

- Scheme 2: $R(0) \tilde{F}'_1 = 1/2 F' = 1$ branching ratio method. Using analogous logic, we find

$$G_0^{(2)} = \frac{(4G_{0+1} - 3) \frac{br_{F=0}}{br_{F=1}} + 1}{1 + \frac{br_{F=0}}{br_{F=1}}}, \quad (5)$$

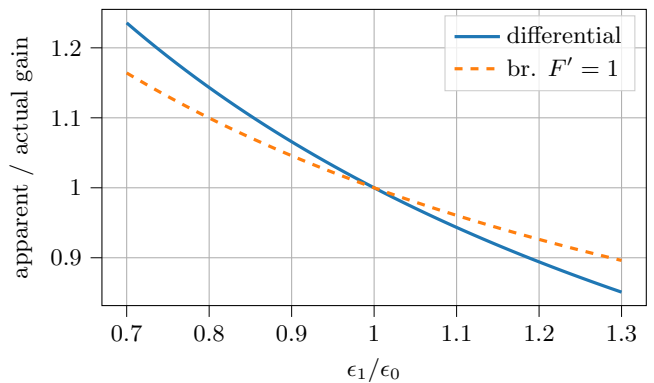


FIG. 5. Dependence of the apparent gain found using the differential method (Scheme 3, Eq. 7) and the $R(0) \tilde{F}'_1 = 1/2 F' = 1$ branching method (Scheme 2, Eq. 5) on the ratio of detection efficiencies for the $J = 0, F = 1$ state, ϵ_1 , and for the $J = 0, F = 0$ state, ϵ_0 . The $F = 0, m_F = 0$ level has on average a smaller contribution to the dark states under different polarizations than the $F = 1$ manifold, resulting in $\epsilon_1/\epsilon_0 < 1$.

where, as before,

$$G_{0+1} \equiv \frac{S_{0+1}^{\text{on}}}{S_{0+1}^{\text{off}}}. \quad (6)$$

Further details are provided in Appendix A.

- Scheme 3: Differential method. This method uses information from both probe transitions, without any need for knowledge of the branching ratios. Here,

$$G_0^{(3)} = 4G_{0+1} - 3G_1. \quad (7)$$

Additional details are given in Appendix A.

From both simulations and measurements, we have found that, for the available laser power and interaction time, the $R(0) \tilde{F}'_1 = 1/2 F' = 1$ transition does not result in the maximum possible number of photons scattered per molecule. We attribute this fact to the existence of dark states in this transition, despite our effort to destabilize these states by rapid polarization switching [12]. This results in small discrepancies between the actual gain and the gain determined with schemes that use $R(0) \tilde{F}'_1 = 1/2 F' = 1$ probe transition, i.e., our schemes 2 and 3. By contrast, the $R(0) \tilde{F}'_1 = 3/2 F' = 2$ transition has no dark states; as such, our scheme 1 provides a more reliable measure of the gain from rotational/hyperfine cooling. The discrepancies in schemes 2 and 3 vary with the relative excitation efficiency for the $J = 0, F = 1$ level (ϵ_1) versus that for the $J = 0, F = 0$ level (ϵ_0): the larger the difference, the larger the apparent gain when determined using schemes 2 and 3. Figure 5 displays this behavior. Additional details are provided in Appendix B.

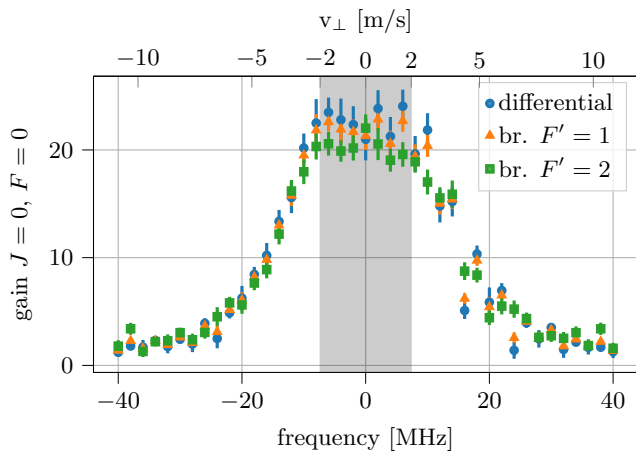


FIG. 6. Gain in the $J = 0, F = 0$ population plotted against the detuning from the central $P(2) \tilde{F}'_1 = 3/2 F' = 1$ line, with a gain of 20.1(4) for the $R(0) \tilde{F}'_1 = 3/2 F' = 2$ branching method, a gain of 22.1(4) for the $R(0) \tilde{F}'_1 = 1/2 F' = 1$ branching method, and a gain of 22.9(6) for the differential method. The grey shaded area corresponds to a detuning equivalent to ± 2 m/s, which is the transverse velocity acceptance range of the electrostatic lens.

IV. RESULTS

Our primary results are shown in Figure 6. Given the drawbacks of employing the $R(0) \tilde{F}'_1 = 1/2 F' = 1$ transition in detecting the rotational cooling gain, as demonstrated in Sec. III E, we only use the result Scheme 1 (based on the branching ratios of the $R(0) \tilde{F}'_1 = 3/2 F' = 2$ transition) for our quantitative conclusions (Eq. 4).

Figure 6 shows the measured gain as a function of laser detuning for the three different methods. Over the central region of transverse velocities, with $|v_\perp| < v_\perp^{\max} \pm 2$ m/s, the gain is independent of v_\perp , with average value $G_0^{(1)} = 20.1(4)$.

The method of Scheme 2 (Eq. 5) resulted in a measured gain of $G_0^{(2)} = 22.1(4)$ and the method of Scheme 3 (Eq. 7) resulted in a measured gain of $G_0^{(3)} = 22.9(6)$. As expected, due to the dark states, this gain differs from the gain of Scheme 1 ($G_0^{(1)}$), and the discrepancy is larger for Scheme 3.

We also monitored the depletion of the various levels excited in the rotational cooling process, and calculated the expected gain based on the degree of depletion. The results (depletion of 85%, 79%, and 81%, respectively, for the $J = 1, 2$, and 3 states) corresponded to an expected gain of $G_0 \approx 24$, broadly consistent with the result of Scheme 1. However, we found evidence that the population of the initially depleted states was modified by the presence of scattered microwaves in the region between the rotational cooling laser beams and the detection laser beam. Hence, we use this information only for qualitative confirmation of our results. Appendix C contains further details.

V. CONCLUSION

We have demonstrated a rotational cooling gain of $G_0 = 20.1(4)$ in the population of the $|J = 0, F = 0\rangle$ state of TlF molecules, sufficient for achieving the projected statistical sensitivity of CeNTREX [1].

From simulations, we expect that increasing the power of the rotational cooling laser to above ~ 500 mW should result in full depletion of the $J = 1, 2$, and 3 states over the relevant velocity range, resulting in a gain of over 25. We are currently implementing a new laser system capable of achieving this power. Another factor of ~ 1.5 improvement in the gain could be obtained by adding a second cooling laser to pump out the $|J = 0, F = 1\rangle$ hyperfine manifold via the $R(0) \tilde{F}'_1 = 3/2 F' = 2$ transition. This transition has no dark states and could be saturated with modest laser power. Together, these improvements could lead to a total gain of nearly 40 and a corresponding statistical improvement in the CeNTREX measurement of the ^{205}Tl nuclear Schiff moment.

ACKNOWLEDGMENTS

We are grateful for support from the John Templeton Foundation, the Heising-Simons Foundation, a NIST Precision Measurement Grant, NSF-MRI grants PHY-1827906, PHY-1827964, and PHY-1828097, NSF grant PHY-2110420, and the Department of Energy (DOE), Office of Science, Office of Nuclear Physics, under contract number DEAC02-06CH11357 and grant number DE-SC0024667.

Appendix A: Detection gain

Throughout this section the following notational conventions are used: ρ_0 (ρ_1) denotes the population in the $F = 0$ ($F = 1$) hyperfine manifold, ρ_0^{RC} (ρ_1^{RC}) is this population after rotational cooling, $n_{\gamma,0}$ ($n_{\gamma,1}$) denotes the number of photons scattered for $F = 0$ ($F = 1$), and G_0 (G_1) is the population gain in the $F = 0$ hyperfine manifold. The signal for a transition is denoted by S , where a superscript of RC indicates a signal after rotational cooling.

The $R(0) \tilde{F}'_1 = 3/2 F' = 2$ transition addresses only the $F = 1$ hyperfine level in the $J = 0$ rotational manifold, and the signal is described as

$$S_{R0F2} = S_1 = \rho_1 \cdot n_{\gamma,1}. \quad (\text{A1})$$

The $R(0) \tilde{F}'_1 = 1/2 F' = 1$ transition addresses the $F = 0$ and $F = 1$ hyperfine levels in the $J = 0$ rotational manifold, and the signal is denoted by

$$S_{R0F1} = S_{0+1} = \rho_0 \cdot n_{\gamma,0} + \rho_1 \cdot n_{\gamma,1}, \quad (\text{A2})$$

where, under the assumption of optical cycling to completion, it can be written as

$$S_{0+1} = (\rho_0 + \rho_1) \cdot n_\gamma. \quad (\text{A3})$$

Further calculations assume that when the population is thermally distributed, it is evenly spread over the hyperfine sublevels of a single rotational manifold, hence $\rho_1 = 3\rho_0$.

With the known branching ratios for the $P(2) \tilde{F}'_1 = 3/2 F' = 1$ transition to each of the $F = 0$ and $F = 1$ hyperfine manifolds, the individual transitions can be used to calculate G_0 . Starting with $R(0) \tilde{F}'_1 = 3/2 F' = 2$:

$$\Delta\rho_1 = \rho_1^{RC} - \rho_1 = \rho_1 (G_1 - 1), \quad (\text{A4})$$

$$\Delta\rho_0 = \frac{br_{F=0}}{br_{F=1}} \Delta\rho_1. \quad (\text{A5})$$

Using $3\rho_0 = \rho_1$ the increase in population to ρ_0 is given by

$$\Delta\rho_0 = 3 \frac{br_{F=0}}{br_{F=1}} \rho_0 (G_1 - 1). \quad (\text{A6})$$

Finally, the gain in $F = 0$ is then given by

$$G_0^{(1)} = \frac{\rho_0^{RC}}{\rho_0} = 3 \frac{br_{F=0}}{br_{F=1}} (G_1 - 1) + 1, \quad (\text{A7})$$

where the superscript refers to the number of the scheme. This is the same result as in Eq. (4).

For $R(0) \tilde{F}'_1 = 1/2 F' = 1$ the gain G_0 can also be calculated with the branching ratios. First we invert Eq. (A7) to get

$$G_1 = \frac{G_0 - 1}{3 \frac{br_{F=0}}{br_{F=1}}} + 1. \quad (\text{A8})$$

Substituting this into Eq. (A12) below, we obtain

$$G_0^{(2)} = \frac{(4G_{0+1} - 3) \frac{br_{F=0}}{br_{F=1}} + 1}{1 + \frac{br_{F=0}}{br_{F=1}}}. \quad (\text{A9})$$

The differential method of calculating the gain uses both transitions. The gain in signal size for each transition can be written as

$$G_1 = \frac{S_1^{\text{on}}}{S_1^{\text{off}}} = \frac{\rho_1^{RC}}{3\rho_0}, \quad (\text{A10})$$

$$G_{0+1} = \frac{S_{0+1}^{\text{on}}}{S_{0+1}^{\text{off}}} = \frac{\rho_0^{RC} + \rho_1^{RC}}{4\rho_0}. \quad (\text{A11})$$

The gain in $F = 0$ is then given by

$$G_0^{(3)} = 4G_{0+1} - 3G_1. \quad (\text{A12})$$

Appendix B: Apparent gain increase

Under incomplete optical cycling of the $R(0) \tilde{F}'_1 = 1/2 F' = 1$ detection transition, a larger apparent gain is measured. This stems from the imbalance between the detection efficiency of the $F = 1$ levels and the $F = 0$ level of the $J = 0$ ground state manifold. The $R(0) \tilde{F}'_1 = 1/2 F' = 1$ transition has 4 ground state levels and 3 excited state levels, meaning there is always a single dark state, for any polarization. The $F = 0, m_F = 0$ level on average has a smaller contribution to the dark states under different polarizations than the $F = 1$ manifold. Due to the increase in population after RC, which predominantly pumps into $F = 0$, a larger fraction of the detected photons per molecule comes from $F = 0$ with rotational cooling than without it. The detection methods employing $R(0) \tilde{F}'_1 = 1/2 F' = 1$ all rely on the ratio between the signal with and without RC ($S_{0+1}^{\text{on}}/S_{0+1}^{\text{off}}$) and this results in a larger ratio than would be expected based on true population increases.

Substituting $\rho_i \epsilon_i$ for ρ_i , using $g = \rho_0^{RC}/\rho_0$ and $\rho_1 =$ in Eq. A11 For a given gain $g = \rho_0^{RC}/\rho_0$, $br_{1/0} = br_{F=1}/br_{F=0}$ and detection efficiencies ϵ_0, ϵ_1 for $F = 0, F = 1$, respectively, the signal ratio for $R(0) \tilde{F}'_1 = 1/2 F' = 1$ can be described by

$$\frac{S_{0+1}^{\text{on}}}{S_{0+1}^{\text{off}}} = \frac{g\epsilon_0 + [3 + (g-1)br_{1/0}]\epsilon_1}{\epsilon_0 + 3\epsilon_1}, \quad (\text{B1})$$

and by the signal ratio for $R(0) \tilde{F}'_1 = 3/2 F' = 2$ can be described by

$$\frac{S_1^{\text{on}}}{S_1^{\text{off}}} = \frac{(g-1)br_{1/0} + 3}{3}. \quad (\text{B2})$$

Equation (7) for calculating the gain from a differential measurement can then be rewritten as

$$G_0^{(3)} = \frac{[3 + br_{1/0}(g-1)]\epsilon_1/\epsilon_0 + 4g - 3 + br_{1/0}(1-g)}{1 + 3\epsilon_1/\epsilon_0}, \quad (\text{B3})$$

and Eq. (5) for calculating the gain from $R(0) \tilde{F}'_1 = 1/2 F' = 1$ with the branching ratios can be rewritten as

$$G_0^{(2)} = \frac{[4br_{1/0}(g-1) + 12] \epsilon_1/\epsilon_0}{(br_{1/0} + 1)(1 + 3\epsilon_1/\epsilon_0)} + \frac{(br_{1/0} - 3)(1 + 3\epsilon_1/\epsilon_0) + 4g}{(br_{1/0} + 1)(1 + 3\epsilon_1/\epsilon_0)}. \quad (\text{B4})$$

The $F = 0, m_F = 0$ level has on average a smaller contribution to the dark states under different polarizations than the $F = 1$ manifold, such that $\epsilon_1/\epsilon_0 < 1$, resulting in an increase in the measured gain for both Eqs. B3 and B4.

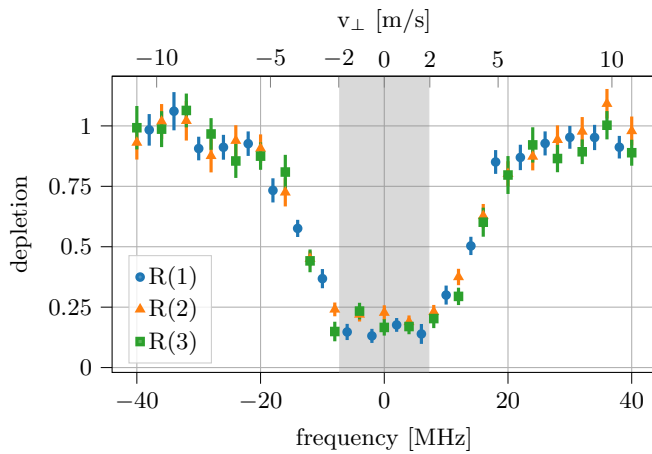


FIG. 7. Depletion for the $R(1) \tilde{F}'_1 = 5/2 F' = 3$, $R(2) \tilde{F}'_1 = 7/2 F' = 4$ and $R(3) \tilde{F}'_1 = 9/2 F' = 5$ transitions, plotted against detuning from the central $P(2) \tilde{F}'_1 = 3/2 F' = 1$ line. Observed depletions are 0.85(2), 0.79(2) and 0.81(2) for $R(1)$, $R(2)$ and $R(3)$, respectively. For $T_{\text{rot}} = 6.3(2)$ K this corresponds to a gain of 24.1(11) in $J = 0$, $F = 0$. The grey shaded area corresponds to a detuning equivalent of ± 2 m/s, which is the transverse velocity acceptance range of the electrostatic lens.

Appendix C: Gain from measured depletion of rotational states

Monitoring the extent to which the population of the rotational levels $J = 1, 2, 3$ is depleted in the rotational

cooling process provides an independent scheme for determining the rotational cooling gain G_0 . The depletions are determined by measuring the $R(1) \tilde{F}'_1 = 5/2 F' = 3$, $R(2) \tilde{F}'_1 = 7/2 F' = 4$ and $R(3) \tilde{F}'_1 = 9/2 F' = 5$ transitions while toggling the RC on/off. Below, d_i corresponds to the ratio between the $R(i)$ transition with RC on and off.+

This method requires an independent knowledge of the rotational temperature, T . We find

$$G_0^{(4)} = 1 + \frac{br_{F=0}}{br_{F=0} + br_{F=1}} \frac{d_1 \rho_{1,T} + d_2 \rho_{2,T} + d_3 \rho_{3,T}}{\rho_{0,T}}, \quad (\text{C1})$$

where $\rho_{i,T}$ and d_i are the thermal population and depletion factor of $J = i$, respectively.

Figure 7 shows the measured depletions, corresponding to loss of population by factors of 0.85(2), 0.79(2) and 0.81(2) for $R(1)$, $R(2)$ and $R(3)$, respectively. This would correspond to a total expected gain of $G_0 = 24.1(1.1)$, assuming $T_{\text{rot}} = 6.3(2)$ K and equal levels of depletion over all hyperfine states in a rotational manifold. As mentioned in the main text, we suspect that the modest discrepancy with the result from our primary measurement method arises because, during these measurements, microwaves leaked into the detection chamber and affected the measured depletion ratios.

-
- [1] O. Grasdijk, O. Timgren, J. Kastelic, T. Wright, S. Lamoreaux, D. DeMille, K. Wenz, M. Aitken, T. Zelevinsky, T. Winick, and D. Kowall, CeNTREX: A new search for time-reversal symmetry violation in the ^{205}Tl nucleus, *Quantum Science and Technology* **6**, 044007 (2021).
 - [2] P. Sandars, Measurability of the proton electric dipole moment, *Physical Review Letters* **19**, 1396 (1967).
 - [3] N. R. Hutzler, H.-I. Lu, and J. M. Doyle, The buffer gas beam: An intense, cold, and slow source for atoms and molecules, *Chemical reviews* **112**, 4803 (2012).
 - [4] X. Wu, P. Hu, Z. Han, D. G. Ang, C. Meisenhelder, G. Gabrielse, J. M. Doyle, and D. DeMille, Electrostatic focusing of cold and heavy molecules for the acme electron edm search, *New Journal of Physics* **24**, 073043 (2022).
 - [5] N. R. Hutzler, M. F. Parsons, Y. V. Gurevich, P. W. Hess, E. Petrik, B. Spaun, A. C. Vutha, D. DeMille, G. Gabrielse, and J. M. Doyle, A cryogenic beam of refractory, chemically reactive molecules with expansion cooling, *Phys. Chem. Chem. Phys.* **13**, 18976 (2011).
 - [6] R. Glöckner, A. Prehn, B. G. U. Englert, G. Rempe, and M. Zeppenfeld, Rotational cooling of trapped polyatomic molecules, *Phys. Rev. Lett.* **115**, 233001 (2015).
 - [7] T. Courageux, A. Cournol, D. Comparat, B. V. de Lesegno, and H. Lignier, Efficient rotational cooling of a cold beam of barium monofluoride, *New Journal of Physics* **24**, 025007 (2022).
 - [8] O. Timgren, *Progress towards a measurement of time-reversal symmetry violation in thallium fluoride*, Ph.D. thesis, Yale University (2023).
 - [9] E. Norrgard, E. Edwards, D. McCarron, M. Steinecker, D. DeMille, S. S. Alam, S. Peck, N. Wadia, and L. Hunter, Hyperfine structure of the $B^3\Pi_1$ state and predictions of optical cycling behavior in the $X \rightarrow B$ transition of TlF, *Physical Review A* **95**, 062506 (2017).
 - [10] G. Meijer and B. G. Sartakov, Λ doubling in the $B^3\Pi_1$ state of TlF, *Physical Review A* **101**, 042506 (2020).
 - [11] L. Hunter, S. Peck, A. Greenspon, S. S. Alam, and D. DeMille, Prospects for laser cooling TlF, *Physical Review A* **85**, 012511 (2012).
 - [12] D. J. Berkeland and M. G. Boshier, Destabilization of dark states and optical spectroscopy in Zeeman-degenerate atomic systems, *Phys. Rev. A* **65**, 033413 (2002).
 - [13] E. S. Shuman, J. F. Barry, D. R. Glenn, and D. DeMille, Radiative force from optical cycling on a diatomic molecule, *Phys. Rev. Lett.* **103**, 223001 (2009).
 - [14] M. Yeo, M. T. Hummon, A. L. Collopy, B. Yan, B. Hemmerling, E. Chae, J. M. Doyle, and J. Ye, Rotational state microwave mixing for laser cooling of complex diatomic

- molecules, [Phys. Rev. Lett. **114**, 223003 \(2015\)](#).
- [15] M. R. Tarbutt, B. E. Sauer, J. J. Hudson, and E. A. Hinds, Design for a fountain of YbF molecules to measure the electron's electric dipole moment, [New Journal of Physics **15**, 053034 \(2013\)](#).